Coverage-dependent structural phase transformations in the adsorption of pentacene on an aperiodically modulated Cu film

M. Lahti and K. Pussi
Lappeenranta University of Technology, School of Engineering Science, P.O. Box 20 FIN-53851 Lappeenranta, Finland.

J. A. Smerdon
Jeremiah Horrocks Institute for Mathematics, Physics and Astronomy, University of Central Lancashire, Preston PR1 2HE, UK.

K. M. Young, H.R. Sharma and R. McGrath
Surface Science Research Centre, University of Liverpool, Oxford St, Liverpool L69 3BX, UK.

Abstract

Surface ordering of pentacene molecules adsorbed on an aperiodic Cu surface has been studied with density functional theory (DFT) and scanning tunnelling microscopy (STM) as a function of coverage. Below 0.73 ML ($5.3 \cdot 10^{13}$ molecule cm^{-2}), the adsorbate structure is row-like with molecular axes aligned with the steps in the Cu structure. Between this coverage and 1 ML ($7.3 \cdot 10^{13}$ molecule cm^{-2}), a structural phase with a checkerboard structure is seen. At higher coverages, a further phase transition to a high-density row structure is seen for most of the film. DFT with vdW functionals is employed to study how the molecule-molecule and molecule-surface interactions evolve as a function of coverage.

Introduction

The study of aperiodic structures and their properties is an area of surface science which continues to evoke interest and attention [1,2]. The interplay of complex aperiodic surface structure and properties (including adsorption), and the relation to electronic structure is relatively unexplored and yet offers a rich testing ground for fundamental ideas of order and symmetry and their influence on physical systems.

Vicinal (highly-stepped, one or more large Miller indices) surfaces have been the focus of some attention in the past decade for their promise in inducing one-dimensional arrangement of adsorbates. However, they are very disordered due to low coordination.

A thin film of Cu on the fivefold surface of Al–Pd–Mn forms a stable, well-ordered structure that is uniaxially commensurate with the aperiodic structure of the substrate [9]. This structure has been analysed using low-energy electron diffraction and is found to consist of a vicinal surface of a body-centered tetragonal (bct) (100) structure. This bct(100) structure has lattice parameters of a = 2. 88 Å , b = 2. 55 Å and c = 2. 88 Å, with the vicinal surface making an angle α of 13.28 ° relative to the a–b plane. [10] This results in a surface with a very dense pattern of steps which is better ordered than any conventional vicinal surface such as Cu(119).

The use of density functional theory (DFT) in combination with advanced experimental techniques has facilitated the investigation of such increasingly complex surface systems. In this study we build on previous results for molecular adsorption on an aperiodically modulated Cu thin film. We use an improved DFT methodology to quantify previously unresolved parameters of the adsorption system and show that this new information allows a simple explanation of the coverage-dependent structural phase transitions observed in the adsorbed molecular overlayer.

Pentacene ($C_{22}H_{14,}$ dimensions, 1.42×0.5 nm, Pn) is an ambipolar organic semiconductor consisting of five linearly bonded benzene rings. It is used as a *p*-type molecule for organic field effect transistors and it has received much attention because of its unusually high intrinsic charge carrier mobility without doping. Significant deviation from a conventional planar adsorption configuration has been reported for Au(110), with mixed edge on / planar phases [3] and for Al(001) with a peculiar V-shaped bending [4]. Otherwise, minor symmetrical bending of the molecule with the central ring closer to the surface has been reported for adsorption on Au(111), [5] Cu(001), [6] Cu(111), [7] and Cu(110) [8] surfaces. The adsorption site on Cu(111) at low temperature was revealed by Lagoute *et al.*[24] using STM. Its interactions with Ag(111) and Cu(111) have also been investigated with x-ray standing waves to determine the adsorption height [30]. It was found that the arrangement of surface steps could influence the orientation of bulk films grown on Si(111) [31]. In the effort to grow thin films of aligned Pn molecules, the use of Cu(119) as a vicinal substrate was explored using low-energy electron diffraction, ultraviolet photoelectron spectroscopy, [32] and scanning tunneling microscopy (STM) [33].

In our previous article [11] we addressed the trends for Pn adsorption by studying the adsorption of anthracene and naphthalene on this aperiodic Cu surface with density functional theory (DFT). Because of limited computational resources we did not use van der Waals (vdW) functionals. In this article we study both the ordering as a function of coverage and bending of a Pn molecule adsorbed on the aforementioned aperiodic copper surface with DFT and STM. DFT with vdW functionals is employed to study how the molecule-molecule and molecule-surface interactions evolve as a function of coverage.

Experimental details

The sample was grown at the Ames laboratory with a nominal composition of $Al_{70}Pd_{21}Mn_9$ and cut perpendicular to a fivefold axis [34]. Pn was evaporated from a Pyrex tube wrapped with a W filament and thermocouple for temperature regulation and Cu was evaporated from a simple filament source consisting of a piece of OFHC Cu wrapped with a W filament. All depositions and data collection were carried out with the sample maintained at room temperature. A variable-temperature Omicron STM was used for collection of STM data. The experimental data presented are collected as detailed earlier [11].

Computational details

The static calculations for total energies were performed using the Vienna ab initio simulation package (VASP) [12-16] including the projector augmented wave (PAW) [17] potentials. A kinetic energy cut-off of 400 eV was applied for the plane waves. The exchange and correlation functionals were treated by the generalized-gradient approximation (GGA) of Perdew–Burke–Ernzerhof (PBE) as proposed by Perdew, Burke, and Ernzerhof [18]. The 8 × 8 × 1 Monkhorst-Pack mesh [19] was used for k-point sampling. The Cu surface was modelled using the supercell approach, where periodic boundary conditions are applied to the central supercell. The surface slab was modelled with 5 layers of Cu. The number of of Cu atoms was between 138 atoms to 299 atoms depending of the coverage and the surface structure. A region of approximately 20 Å of vacuum was inserted in the *z*-direction to prevent interactions occurring between periodic images. The bottom layer of the surface slab was fixed during geometry relaxation. For the description of long-range vdW energy the optB86b-vdW functional [20] was used. This functional gives the experimental lattice constant for Cu and also gives good agreement for the adsorption energy of benzene on Cu surfaces [21,22].

The adsorption energies of molecules are defined as:

$$E_{ads} = \frac{1}{N}\left(E_{tot} - E_{clean} - N\,E_{mol}\right) \qquad (1)$$

where E_{tot} is total energy of a relaxed supercell with molecules, E_{clean} is the total energy of the relaxed clean Cu slab, N is the number of molecules and E_{mol} is the energy of one molecule in the space.

In the calculation of Pn adsorption sites two different supercells are used: one with 138 atoms and the other with 184 atoms. The number of surface Cu atoms was 30 and 40 respectively. The smaller supercell was mainly used to reduce the level of computational resources required. From the starting configuration, full relaxation of the atomic positions was allowed until the forces were minimized. In the relaxed configuration, the molecule lies flat on the surface.

Results

Clean Fibonacci modulated copper surface

The Fibonacci modulated Cu surface contains two different kinds of fcc(100) oriented terraces: long (L) and short (S), separated by fcc(111) oriented steps and arranged in a binary Fibonacci sequence (LSLLS...). The film grows in layers parallel to the substrate and contains inter-layer steps; henceforth we differentiate the intra-layer fcc(111) oriented steps by referring to them as Fibonacci rows, and to the overall structure as the Fibonacci row structure. Long terraces are three atomic rows wide and short terraces are two atomic rows wide. The density of surface Cu atoms is around 63% of that of a Cu(100) surface, though it is not as well defined for this complicated surface. The Fibonacci row structure is very dense (L=7.3 Å, S=4.5 Å), therefore, each adjacent row cannot be decorated by an unbroken chain of molecules. [11] This surface is therefore unique in at least two regards: first, it is aperiodic, in the sense that a periodic structure is perturbed by an aperiodic modulation; and second, it is vicinal, in the sense that there is a well-defined cut plane across an underlying periodic structure. As it is also flat and well-ordered, it differs from other vicinal surfaces which are usually quite disordered due to low coordination.

The structure is inherently three-dimensional, exhibiting lesser coverage with each additional layer, resulting in a sparse top layer of Cu islands atop at least one more layer with gaps, in turn atop at least one continuous layer of Cu covering the substrate. Despite this, the film is predominantly flat, with much more of the Cu surface parallel to the substrate surface than is occupied in forming steps. We focus on adsorption on the `flat' Cu surface and neglect stepwise adsorption, which is likely to show the same tendency as for any other stepped surface.

The relaxation of this Cu surface was previously studied using DFT without taking into account the vdW interactions. These calculations indicated that the symmetry of the clean surface remained almost constant, though the edge row of the longer terrace falls slightly [11]. In the case of calculations with vdW functionals, surface distortion occurs during relaxation of the clean surface. The lattice constant of Cu found with the optB86b-vdW functional is convergent with the experimental lattice constant which makes this result more reliable than in the case of calculations without vdW functionals. [29] In the distortion the edge row of the longer terrace moves to a new position and causes modifications to the whole surface. However, the largest change is a gap between the second and third row of the longer terrace, which makes the L terraces locally wider (resembling Cu(110)) and probably increases the reactivity at this local site. The distance between the second and the third atomic row on L terraces before and after surface distortion is 2.9 Å and 3.6 Å, illustrated in Figure 1.

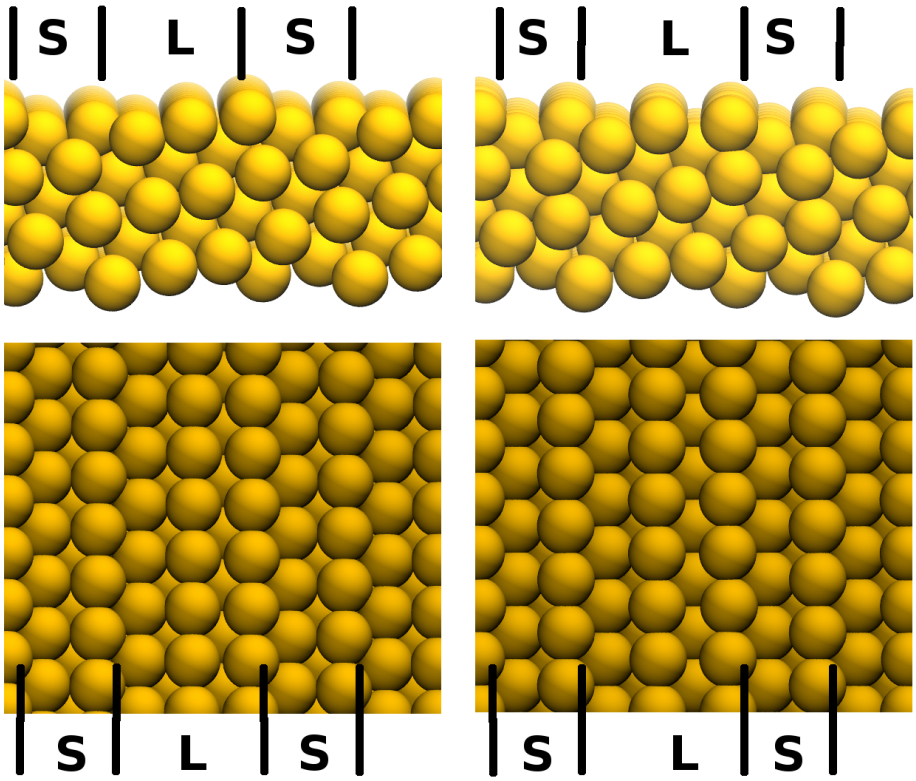

Fig. 1: a) Side view of the model surface before relaxation. c) Top view of the surface before relaxation. b) Side view of the distorted surface .d) Top view of the distorted surface.

Pn adsorption

Coverage definition

The use of monolayers (ML) as a unit of coverage is intuitive, though not very transparent when there are density-related phase transitions in a molecular overlayer. For this reason, our earlier report uses the unit of molecule cm^{-2} [11]. However, the definition of 1 ML as the coverage at which the number of C atoms in adsorbed Pn molecules is the same as the number of surface Cu atoms is intuitive and convenient for describing DFT results and is also the coverage at which the checkerboard structure observed previously [11] and examined here is saturated. To take advantage of both schemes, we present coverages side-by-side in both ML and molecule cm^{-2}, with 1 ML equal to $7.3 \cdot 10^{13}$ molecule cm^{-2}.

Scanning tunneling microscopy

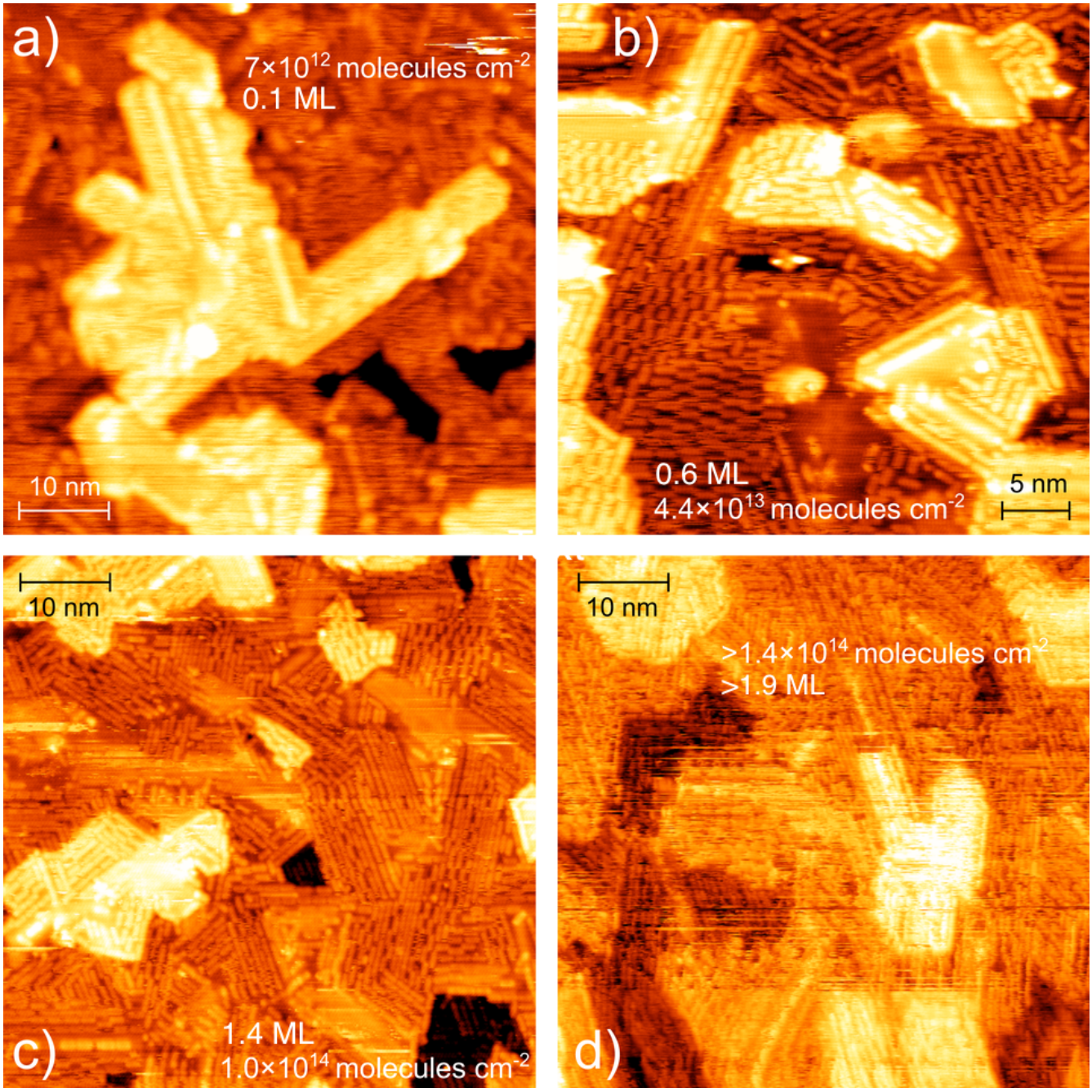

Fig. 2: Room temperature scanning tunneling microscopy of the evolution of the Pn structure with coverage. Quoted coverages are estimated to be accurate within 10%. Quoted voltages are sample bias. Data are unprocessed except for leveling and a false color map. (a) 60 nm × 60 nm, I_T=0.11 nA, V_B=1.03 V. The linear features are end-to-end Pn rows. Between some of these rows are parallel rows with significant noise, which indicates there are mobile pentacene molecules on the surface. (b) I_T=0.087 nA, V_B=-1.14 V. The checkerboard pattern is clearly visible. Noise is greatly reduced. Another STM image of this area is published in [11]. (c) I_T=0.1 nA, V_B=-1 V. The checkerboard pattern no longer dominates and more Pn molecules are lined up in a row structure. (d) I_T=0.1 nA, V_B=-1.3 V No checkerboard structure is visible. The data are very noisy due to the diffusion of loosely bound second layer molecules.

In Figure 2 we present STM data collected from this system at various coverages. The islands observed in the STM topographs are Cu islands, due to the three-dimensional nature of the Cu growth mode, rather than islands of pentacene molecules, which are observed individually as rods of approximately 2 nm × 0.4 nm. Coverages are obtained by counting molecules and are approximate due to the nonuniformity of the coverage and the occasional lack of definition in the molecules. The largest source of error is the indistinctness of the molecules, which we estimate leads to an error of approximately 10%. Counting is done on STM data where the molecules are resolved, i.e., when some of the surface is covered with the checkerboard structure, which presents a comparison both for uncovered surface and for surface covered by the row structure, which are for the most part indistinguishable otherwise. Coverages are estimated based on deposition time for images without visible checkerboard structure. Due to the patches of Cu free of Pn molecules observed in all our data, even if all of the Pn molecules are in the checkerboard structure, the coverage is less than the maximum checkerboard coverage of 0.98 ML or $7.1 \cdot 10^{13}$ molecule cm^{-2}.

The noise evident in the topographs is due to loosely bound molecules moving through some combination of thermal diffusion and interaction with the STM tip. This noise is particularly evident in panel (a), where coverage is very low. Several features are apparently noise-free, notably steps in the Cu film and long end-to-end rows of Pn molecules, which are locations where Pn motion is restricted due to increased coordination with Cu or with coadsorbates. In panel (b), less noise is evident, as most of the available sites for Pn adsorption are occupied, which has the effect of "locking in" the structure. Some portions of the aperiodic Cu substrate are completely clear of Pn molecules, for reasons which are not apparent. Nearly all of the molecular film, however, is in the checkerboard structure described previously [11]. As coverage increases between panels (b) and (c), we see a reduction in the proportion of material manifesting the checkerboard structure.

Since we have no reason to expect that material has desorbed, we find it reasonable to extrapolate that the lack of checkerboard material observed in panel (d) indicates a transformation to some other structure. The STM data point to a return to the row structure but with a tighter inter-row packing. Certain areas appear free of Pn molecules but as they appear to be at the height of the neighboring Pn molecules, we suggest that they are in fact closely packed Pn molecules which are not resolved. There is very little noise in this image, supporting the idea that with increasing coverage, the mobility of Pn molecules is restricted. What noise is observed is higher in *z* than adjacent data, suggesting that it is due to the nascent second layer. In panel (d) coverage is too high to accommodate all molecules in the first layer, as indicated by the large degree of noise originating in the diffusion of second-layer molecules.

If we consider a two-dimensional model system consisting of rigid, round-ended, finite width, finite breadth, elongated three-dimensional batons aligned along their long axes on a set of parallel lines with a separation comparable to the baton dimensions, a checkerboard packing provides both the maximum density and the maximum nearest-neighbor distance of batons. This is sufficient reasoning to understand the adoption of the checkerboard structure, given the attraction to the substrate and the close-range intermolecular repulsion of the Pn molecules, regardless of any additional substrate-mediated repulsion found in previous work [11].

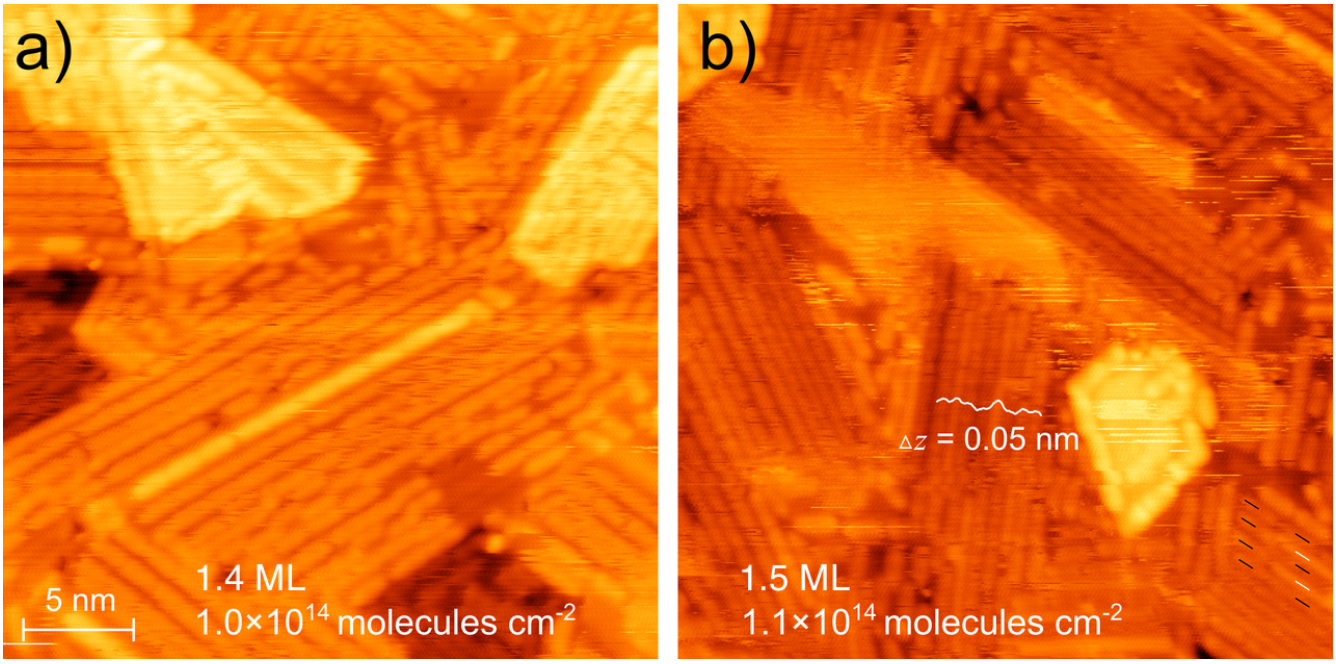

Fig. 3: 30 nm × 30 nm topographs of the Pn/Cu/AlPdMn surface. a) I_T=150 pA, V_B = 1.6 V. Checkerboard structure has been almost completely replaced by another row structure. Noise is observed around some molecules in the remaining checkerboard structure, indicating that these molecules have become unstable in this adsorption configuration. b) I_T=110 pA, V_B = 1.05 V. Slightly higher coverage. No checkerboard Pn remains. The differing heights of the Pn rows shown in the profile are likely to be evidence of tilted rows as explained in the text. Δz given is between the tops of adjacent rows and does not include the Pn layer thickness. In the lower right portion of the image, a transition between 4 flat rows and 3 flat + 2 tilted rows in the same cross-rows distance is indicated. An additional example is shown in the upper middle portion, where 3 flat rows have a small section with an additional tilted row inserted.

In Figure 3 we focus on the second phase transition: the transition from checkerboard to another row structure. However, it is clear that the row structure following the second phase transition contains a higher density of Pn molecules than that preceding the first phase transition. In addition, as highlighted in the center of panel (b), not all rows are of the same height as image via STM. In the lower right portion of panel (b), the black and white dashes indicate a region where a row structure of 4 dim transitions to a structure of 3 dim and 2 bright in the same cross-rows distance. These pieces of information indicate freedom of the molecules to tilt into the third dimension and thus reduce their surface footprint. This process enables molecules to adsorb on more Fibonacci rows and thus to increase the film density. This is the second phase transition.

The second phase transition seems that it can occur with relatively little disruption to the film. The first phase transition involves a large-scale reorganization. We expect that this reorganization energy cost is absorbed by the thermal energy which the molecules already possess, as can be seen from the ready diffusion of the molecules at this temperature.

Density functional theory with van der Waals

Pn adsorption sites

The sites considered for Pn adsorption were selected based on our previous study [11] and the geometry of the surface. In all cases, adsorption crosswise to the Fibonacci rows was less favorable than adsorption parallel to the rows. We include the results for crosswise adsorption in the Supporting Information.

The sites for parallel adsorption are shown in Figure 4 and the associated adsorption energies in Table 1. A larger negative energy indicates a stronger attraction. The best adsorption sites on the smaller supercell (1 and 5) were also tested with the larger supercell, along with adsorption site 4 in order to give another reference point. The adsorption sites in the figures are plotted before and after relaxation except for the sites 8, 9, and 10, which are missing the after geometry as the molecules on these sites drifted away from their before geometries. Pn molecules starting from the sites 9 and 10 drifted to the site number 1, and from site 8 drifted to site number 5.

The top 3 adsorption sites are 1, 11 and 5. 1 and 11 are translated approximately 0.5 Cu NN. The similarity in adsorption energy of these two sites indicates a low barrier for diffusion along the Fibonacci rows. The post-relaxation Fibonacci L-row resembles the Cu(110) surface, and site 11 is chosen as it corresponds to the best adsorption site on the Cu (110) surface [28].

Adsorption site	**Ads. Energy (eV) 0.733 ML $5.3 \cdot 10^{13}$ molecule cm^{-2}**	**Ads. Energy (eV) 0.55 ML $4 \cdot 10^{13}$ molecule cm^{-2}**
1	-4.36	-4.72
2	-3.15	
3	-3.67	
4	-3.14	-3.70
5	-3.73	-4.18
6	-3.29	
7	-2.83	
8	Not stable	
9	Not stable	
10	Not stable	
11	-4.06	-4.44

Table 1: Adsorption energies for the adsorption sites shown in Figure 2. The two righthand columns refer to the two different sizes of Cu slab used in the calculation.

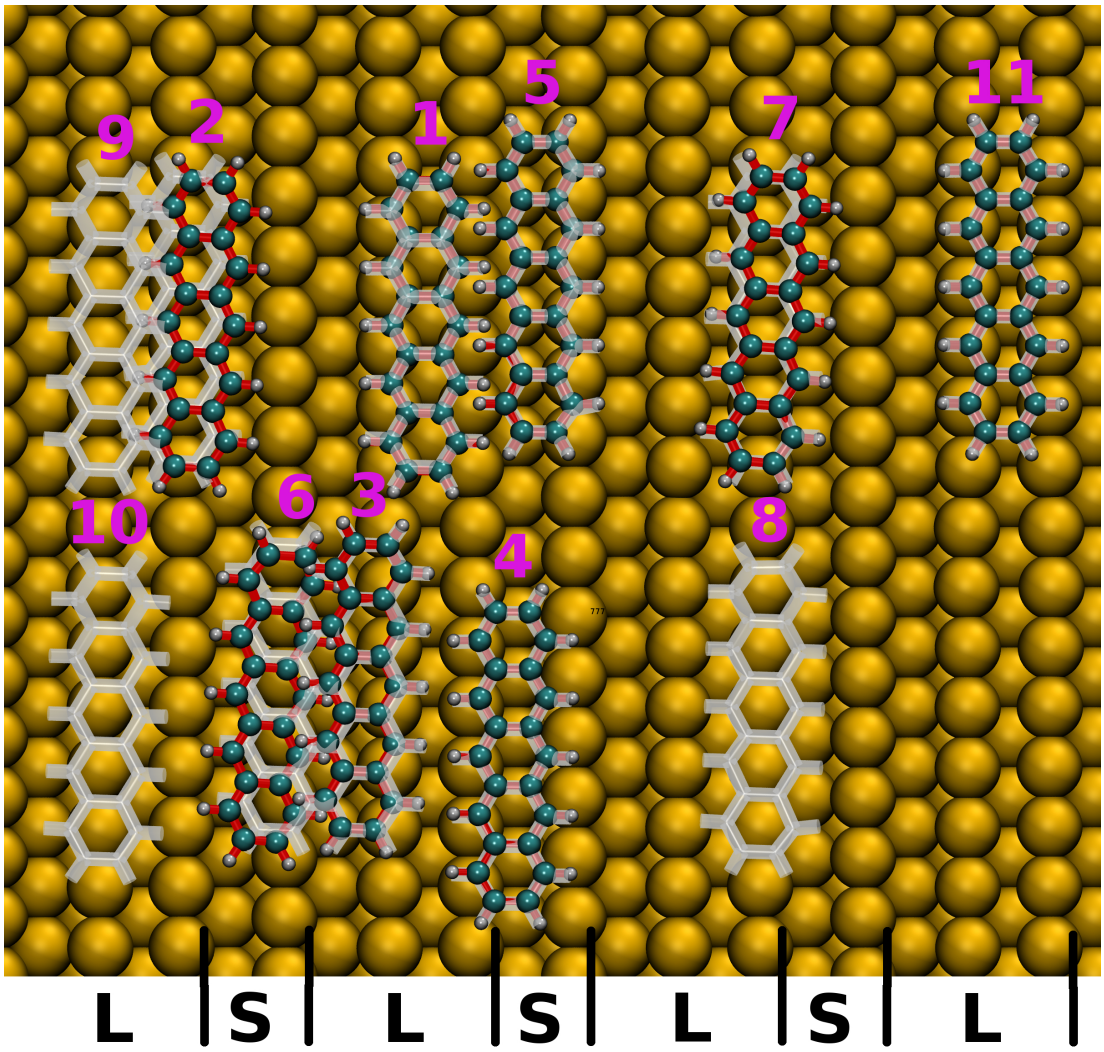

Fig. 4: Adsorption sites. Adsorption energies are listed in Table 1.

Surface structures as a function of coverage

As coverage is varied, the superstructure of the Pn layer changes. As the STM data show, this change is not continuous but has three main phases separated by two phase transitions. When the coverage is low enough, all the molecules stick to the energetically most favorable adsorption sites as expected. In this situation we do not observe via DFT any interaction between the molecules. When coverage is increased and all of the most favorable sites are occupied, the molecules start to occupy the next available best adsorption sites. Placing the molecules at the simultaneously available two most favorable sites produces the checkerboard structure observed previously[11] and here by STM. The calculated checkerboard structure at a coverage of 0.98 ML ($7.1 \cdot 10^{13}$ molecule cm^{-2}) is shown in fig. 5.

The first superstructure phase transition occurs as coverage exceeds 0.73 ML ($5.3 \cdot 10^{13}$ molecule cm^{-2}). Below this coverage the row structure is observed as the molecule can adopt the best adsorption sites. Above this coverage the checkerboard structure is energetically most favorable. The intermolecular

repulsion starts to overwhelm the surface attraction as the coverage increases from 0.55 ML ($4 \cdot 10^{13}$ molecule cm^{-2}) to 0.73 ML ($5.3 \cdot 10^{13}$ molecule cm^{-2}), reflected in the decrease in magnitude of the per-molecule adsorption energy. It is impossible to maintain a flat-lying row structure with coverage above 0.73 ML ($5.3 \cdot 10^{13}$ molecule cm^{-2}) because after that molecules start to overlap with each other.

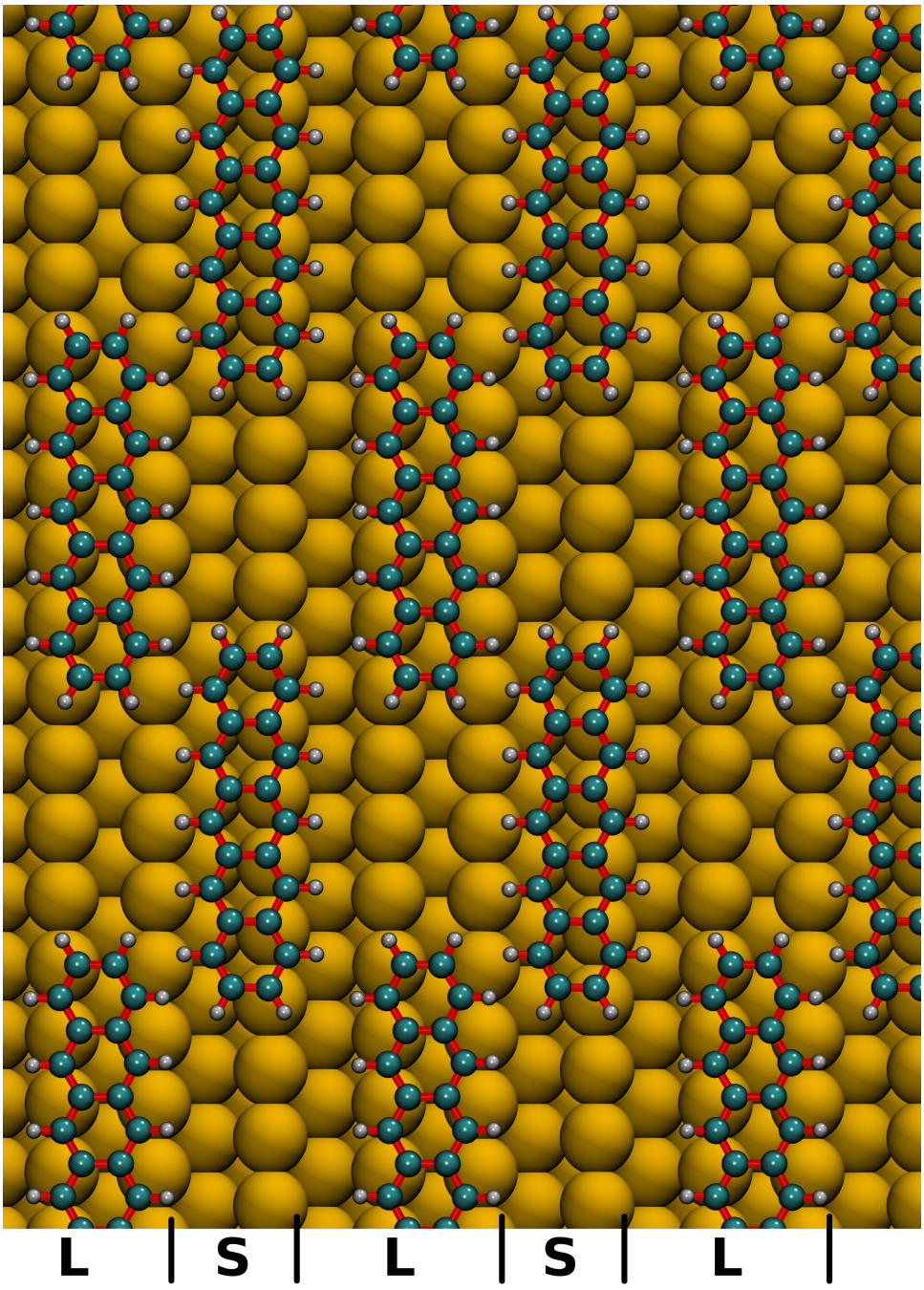

Fig. 5 Calculated checkerboard structure with coverage of 0.98 ML ($7.1 \cdot 10^{13}$ molecule cm^{-2}) .

Tilted rows

Raising the number of molecules beyond that which can fit in a checkerboard structure (0.98 ML / $7.1 \cdot 10^{13}$ molecule cm^{-2}) leads to a tilted row structure. This is the second phase transition. DFT simulations are run for coverage of 1.46 ML ($1.1 \cdot 10^{14}$ molecule cm^{-2}) as shown in Figure 10. This high coverage structure illustrates a situation where all Fibonacci rows are occupied and on each Fibonacci row the Pn molecules are as close as they can get. The shortest vertical distance between the C atoms of the Pn molecule and the Cu atoms of the substrate is 2.2 Å for both L and S Fibonacci rows. The

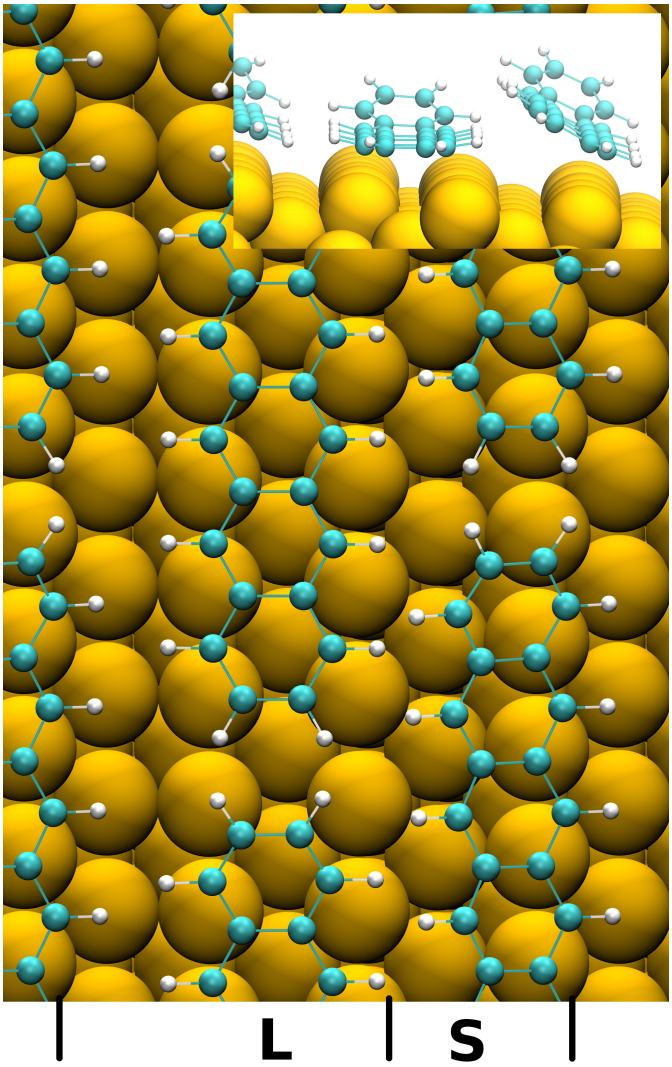

Fig. 6: Calculated high coverage structure with coverage of 1.46 ML . The insert shows the tilting of the Pn molecule.

distance between the Pn molecules measured between the H atoms is 2.0 Å for the molecules on the same terrace and 2.2 Å for the molecules that are on different terraces. In addition to the bending of the Pn molecules, we also see tilting of about 30 degrees of the molecules that sit on the S-terrace.

The adsorption energy also varies with the coverage. The most negative per-molecule values are observed for low coverage. For the checkerboard structure at coverage at 0.73 ML ($5.3 \cdot 10^{13}$ molecule cm^{-2}) the adsorption energy was -4.40 eV. The adsorption energy of Pn on Cu(111) [7] is calculated, using the same method, as -3.17 eV. This indicates that the bonding between the Fibonacci modulated surface and the molecule is stronger than that for a flat surface.

In the case of the Fibonacci modulated Cu surface it is hard to unambiguously define the adsorption height, so we measure the smallest C-Cu distance, which is 2.1 Å for adsorption site 1. On the Cu(111) surface the distance between the molecule and the surface is experimentally measured to be 2.34 Å [30]. The shorter adsorption height for our surface also supports the assumption of stronger bonding.

Bending of Pn molecule

On low Miller index Cu planes the Pn molecule experiences a bending that can clearly be seen with STM [6,8,23-26] and atomic force microscopy (AFM) [27]. The bending of an isolated Pn molecule has also been quantified using DFT [4,6,7,26]. The bending on the Cu(001) surface is approximately 0.4 Å measured between the center of the molecule and a plane bisecting the H atoms at either ends [8], and on Cu(100) and Cu(111) surfaces the values are 0.16 Å and 0.2 Å measured between the center of the molecule and a plane bisecting the C atoms at either ends [6,7]. Al(001) shows a larger value for bending with peculiar V-shape, where the height difference between the peripheral and central carbon atoms is 1.24 Å. [4] The bending of Pn molecules seems to be driven by something in addition to optimizing C-Cu distance, as 'chain-like' behavior is observed atop Cu(111), where one end of a molecule in a closely-packed layer is forced beneath the end of a neighboring molecule, causing it to tilt and propagate the effect to the next neighbor. Bending is also observed for molecules in the second layer [26].

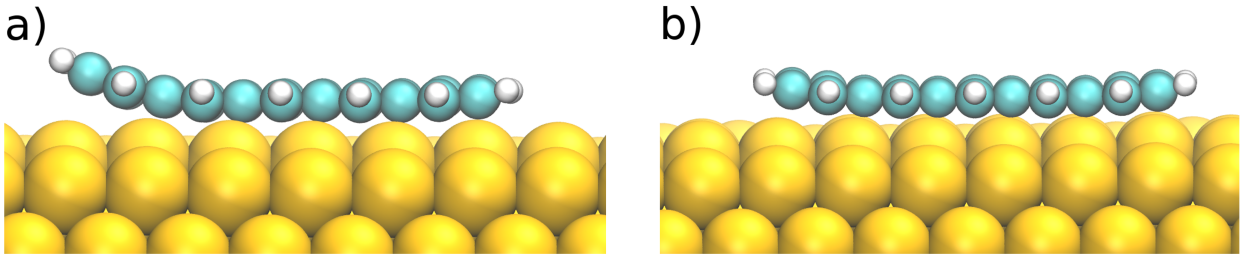

Fig. 7: Bending of the Pn molecule at a coverage of a) 0.733 ML ($5.3 \cdot 10^{13}$ molecule cm^{-2}) and b) 0.40 ML ($2.9 \cdot 10^{13}$ molecule cm^{-2}).

Figure 7 shows side views of Pn bending at two different coverages. Table 3 shows parameters derived from DFT related to the bending of the Pn molecule on Fibonacci modulated copper surface with different coverages (see Figure 7 for a graphical explanation of the different parameters). Bending is measured between the center of the molecule and a plane bisecting the C atoms at either ends of the molecule (surface plane is not unambiguous to define). Table 3 also shows bending measured between the center of the molecule and a plane bisecting the H atoms at either ends. Although the bending of Pn molecules can usually be seen via STM, the noise in our images make a measurement intractable. However, in the image in figure 3 (b), the molecules in the rows have slightly increased definition, which could be a manifestation of this bending.

Coverage (ML(·10^{13}molecule cm^{-2}))	**Distance y (Å)**	**Distance (Å)**	**z1(Å)**	**z2(Å)**	**za(Å)**	**Hz1(Å)**	**Hz2(Å)**	**Hza(Å)**	**D(Cu-C) (Å)**	**Ah(Å)**
0.34 2.4	19.15	19.15	0.32	0.18	0.25	0.58	0.45	0.52	2.203	2.077
0.37 2.7	16.59	16.59	0.34	0.23	0.29	0.57	0.47	0.52	2.209	2.081
0.40 2.9	14.04	14.04	0.35	0.21	0.28	0.55	0.44	0.50	2.228	2.061
0.44 3.2	11.43	11.43	0.36	0.21	0.29	0.53	0.40	0.47	2.225	2.053
0.49 3.5	8.87	8.87	0.28	0.25	0.27	0.51	0.44	0.47	2.239	2.069
0.55 4.1	6.29	6.29	0.41	0.21	0.31	0.59	0.43	0.51	2.227	2.083
0.733 5.3	1.45	1.78	0.89	0.16	0.53	1.23	0.32	0.78	2.191	2.091

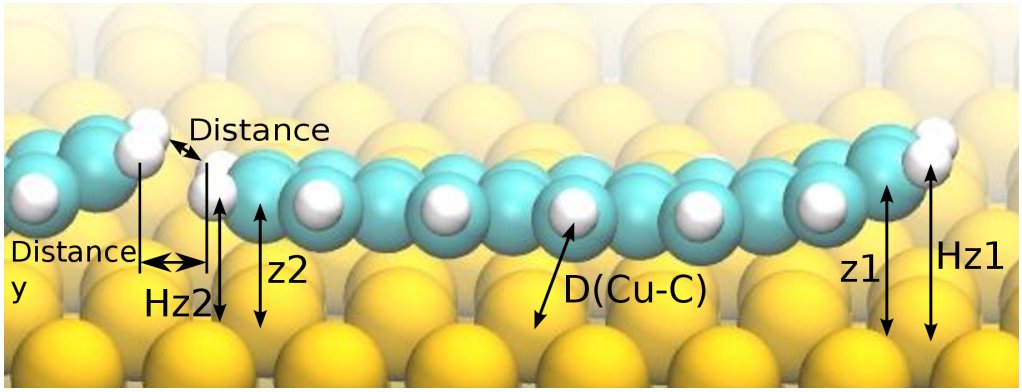

Fig. 8: Graphical explanation for the parameters in Table 4.

Table 2: Parameters related to the bending of the Pn molecule as a function of coverage. Column z1 represents one end of the molecule and column z2 represents another end of the molecule. Column z represents the average value of z1 and z2. Columns Hz1, Hz2 and Hza correspond to the columns z1, z2 and za. Column D(Cu-C) represents a shortest distance between C in the molecule and Cu atom at the surface (bond length). Column Ah represents the average height of the C atoms measured from the row of highest atoms of the surface. See Figure 8 for graphical explanation of the different parameters.

Columns *Distance y* and *Distance* in Table 3 show the distances between the molecules in two different way. First one (*distance y*) means the lateral distance between H atoms of the neighboring molecules. The other (*distance*) is the true distance between the last H atom of the molecule and the first H atom of the next molecule. The only coverage where those two measures are different is 0.733 ML ($5.3 \cdot 10^{13}$ molecule cm^{-2}). At this coverage there is a strong bending of one end of the molecule that affects the real distance. At this coverage the molecules are very close to each other and this clearly causes unusual bending. Repulsion between the ends of the molecules forces a chain effect where one end of a molecule bends up and one end of a neighbouring molecule bends down, as observed for Cu(111) [26]. This causes an overall decrease in adsorption energy.

With lower coverages the bending decreases but there is still some variation. Bending seems to be extremely sensitive to changes in the electrical environment – especially considering that the bending difference between the ends of the molecules varies between molecules.

Figure 9. demonstrates the effect of bending on bonding of the molecule by local DOS plots for C and Cu atoms at different positions related to the molecule. This figure clearly shows that the bonding is strongest in the middle part of the Pn molecule. The bending weakens the bonding so that the higher the molecule end bends the weaker the bonding. However the lower end of the bent molecules bonds more strongly to the surface than the end of unbent molecules in low coverage. This is because the distance between the lower end of the bended molecule and the substrate is smaller than the distance between the end of unbent molecule and the substrate. On average, the bonding in bent molecules is stronger when the bending is asymmetric.

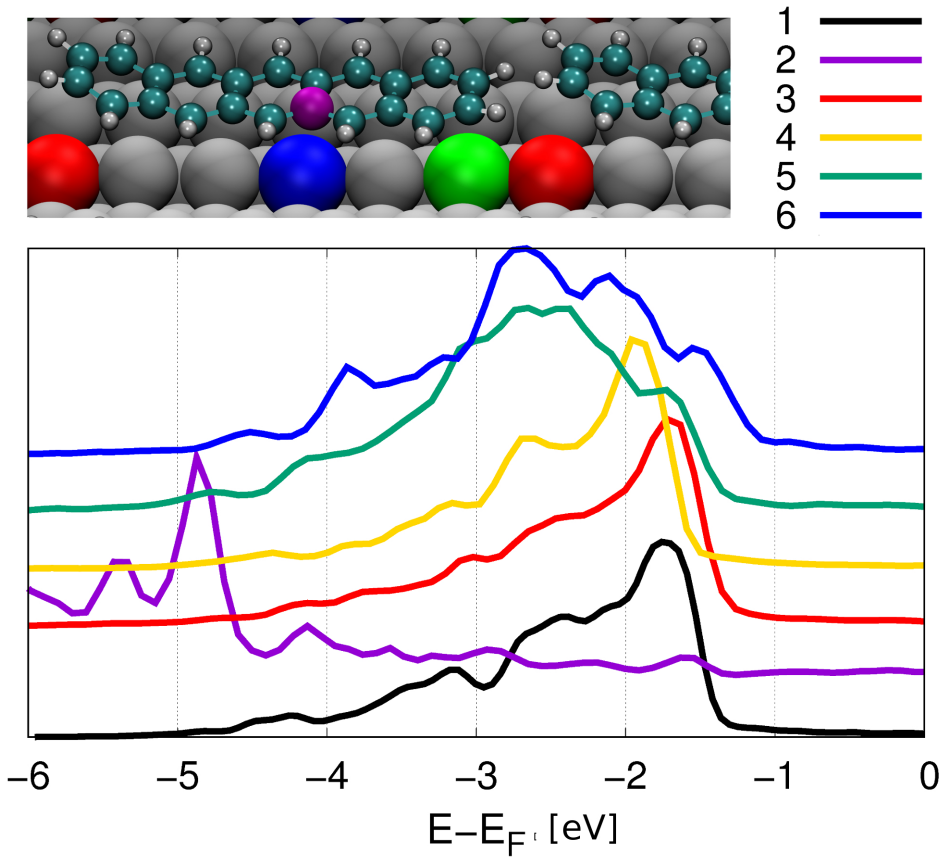

Fig. 9: Local DOS for C and Cu atoms in the row structure. The Pn coverage is 0.733 ML ($5.3 \cdot 10^{13}$ molecule cm^{-2}) for all cases except 1 and 4. 1: Local DOS for a surface Cu atom of the clean substrate. 2: Local DOS of a C atom in the middle part of Pn molecule. 3: Local DOS for a surface Cu atom below the more bent end of the Pn molecule. 4: Local DOS for a surface Cu atom below the end of the Pn molecule at coverage of 0.37 ML ($2.7 \cdot 10^{13}$ molecule cm^{-2}).5: Local DOS for a surface Cu atom below the less bent end of the Pn molecule. 6: Local DOS for a surface Cu atom below the middle part of the Pn molecule. Inset: key showing which atoms the curves correspond to. The yellow curve does not have an associated atom in this diagram because it is for a different coverage.

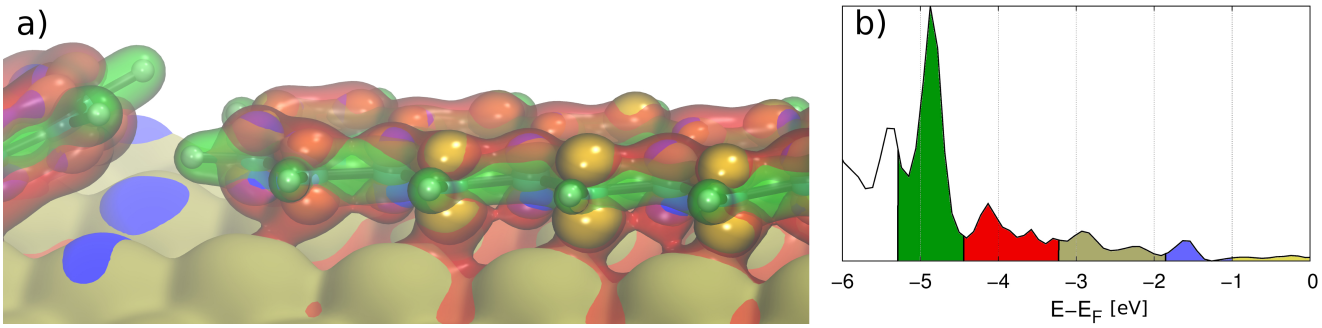

Fig. 10: a) 3-dimensional plot of partial charge density of the Pn molecule on the adsorption site 1 with coverage 0.733 ML ($5.3 \cdot 10^{13}$ molecule cm^{-2}). b) LLocal DOS of a C atom in the middle part of Pn molecule (same curve as in Figure 9). The colored energy regions (-1 – 0 eV yellow, -1.8 - -1 eV blue, -3.2 - -1.8 eV tan, -4.5 - - 3.2 eV red and -5.2 - - 4.5 eV green) correspond to the color coding in partial DOS in figure a)

Figure 10 shows a three-dimensional plot of the partial charge density of a Pn molecule on adsorption site 1 with coverage 0.733 ML ($5.3 \cdot 10^{13}$ molecule cm^{-2}). The coloured energy regions (-1 – 0 eV yellow, -1.8 - -1 eV blue, -3.2 - -1.8 eV tan, -4.5 - - 3.2 eV red and -5.2 - - 4.5 eV green) correspond to the colour coding in partial DOS in figure a).

This clearly shows that bonding is strongest at -4.5 - - 3.2 eV (red). This is the energy region towards which the Cu DOS in Figure 9 spreads in the case of Cu atoms that are close to C atoms. Surprisingly the energy region -1 - 0 eV (yellow) also shows weak bonding even if there is almost no charge for Cu or C in this region. Energy region -1.8 - -3.2 (tan) does not show bonding to the molecule, even if most of the charge for Cu remains in that region. Energy region -4.5 - -5.2 shows no bonding to the surface, although most of the C charge remains at that region.

Figure 10 also illustrates that the more bent end of the molecule does not bond to the surface. This same thing is illustrated in Figure 9 where the DOS for a Cu atom below the more bent end of the molecule remains similar to the DOS of clean surface Cu. i.e. the curve 3 in Figure 9 is not spread towards the -4.5 - - 3.2 eV (red) energy region.

At the chosen energy regions we do not see any bonding between the molecules.

Table 3 lists adsorption energies as a function of the coverage. A more negative adsorption energy for a structure is associated with a greater preference for that structure. Column “row” shows the adsorption energies for one molecule, when only the best adsorption sites are occupied by Pn. Column “checkerboard” shows the adsorption energy for one molecule when the molecules are on adsorption sites 1 and 5. The checkerboard energies are the averages of the adsorption energies of those two sites. For the coverages of 0.37 ML ($2.7 \cdot 10^{13}$ molecule cm^{-2}) and 0.34 ML ($2.4 \cdot 10^{13}$ molecule cm^{-2}), the distances between the molecules in the direction across Cu steps are 16.59 Å and 19.15 Å. The distance between the molecules in the other direction is in both cases 7.42 Å. In this case all distances are measured between the nearest H atoms. The identical adsorption energy indicates that these coverages are below the threshold for intermolecular interaction. Column “tilted row” shows the energy for the densest structure, achieved when molecules develop a tilt along their long axis, allowing them to decorate more rows. The “total adsorption energy” is the product of the number of molecules and each individual adsorption energy. This provides a useful indicator that the overall energy becomes more negative with increasing coverage throughout all phases.

Coverage, ML $\cdot 10^{13}$ molecule cm^{-2}	**Adsorption energy (eV) row**	**Adsorption energy (eV) checkerboard**	**Adsorption energy (eV) tilted row**	**Total adsorption energy ($\cdot 10^{13}$ eV cm^{-2})**
0.34 2.4	-4.75			-11.4
0.37 2.7	-4.75			-12.8
0.40 2.9	-4.74			-13.7
0.44 3.2	-4.74			-15.2
0.49 3.5	-4.73			-16.6
0.55 4	-4.72	-4.40		-18.8 -17.6
0.73 5.3	-4.36	-4.40		-23.1 -23.3
0.80 5.8		-4.32		-25.1
0.88 6.4		-4.25		-27.2
0.98 7.1		-4.06		-28.8
1.10 8		-3.82		-30.4
1.46 11			-3.65	-40.2

Table 3: Adsorption energies as a function of coverage.

Conclusions

We have used DFT and STM to comprehensively investigate and model all stages of the growth of the first layer of pentacene molecules on a Fibonacci modulated Cu film. Molecules have a strong preference to decorate sites which allow them to orient their long axes parallel to the Fibonacci row structure in the Cu film. As coverage is increased the molecules in the row structure get closer together, and the resulting steric effect causes enhanced bending on the molecules. Repulsion between the ends of the molecules forces a chain effect where one end of a molecule bends up and one end of a neighboring molecule bends down, as observed for Cu(111) [26]. This in turn weakens the molecule-surface interaction. The transition from the row structure to the checkerboard structure observed previously [11] takes place at the critical coverage of 0.73 ML ($5.3 \cdot 10^{13}$ molecule cm^{-2}). After all the film has transformed to the checkerboard structure, additional Pn molecules result in a further phase transition to a tilted row structure, observed in STM and DFT. These phase transitions are facilitated by the easy lengthwise sliding of molecules, shown experimentally and using DFT.

Acknowledgements

The EPSRC is thanked for funding under Grant No. EP/D05253X/1 and Academy of Finland for funding under projects #277829 and #218186. CSC - IT Center for Science is thanked for the computational resources.

References

1. J. A. Smerdon, K. M. Young, M. Lowe, S. S. Hars, T. P. Yadav, D. Hesp, V. R. Dhanak, A. P. Tsai, H. R. Sharma, R. McGrath, Nano Lett., **14** (2014) 1184-1189.
2. H. R. Sharma, K. Nozawa, J. A. Smerdon, P. J. Nugent, I. McLeod, V. R. Dhanak, M. Shimoda, Y. Ishii, A. P. Tsai, R. McGrath, Nature Comm., **4** (2013) 2715.

3. G. Bavdek, A. Cossaro, D. Cvetko, C. Africh, C. Blasetti, F. Esch, A. Morgante, L. Floreano, Langmuir **24** (2008) 767−772.
4. A. Baby, G. Fratesi, S. R. Vaidya, L. L. Patera, C. Africh, L. Floreano,and G. P. Brivio, J. Phys. Chem. C **119** (2015) 3624−3633.
5. P. Schroeder, C. France, J. Park, B. Parkinson, J. Appl. Phys. **91** (2002) 3010−3014.
6. A. Ferretti, C. Baldacchini, A. Calzolari, R. Di Felice, A. Ruini, E. Molinari, and M. G. Betti, Phys. Rev. Lett. **99** (2007) 046802 .
7. X-Q. Shi, Y. Li, M. A. Van Hove, R-Q. Zhang, J. Phys. Chem. C, **116** (2012) 23603.
8. K. Müller, A. Kara, T.K. Kim, R. Bertschinger, A. Scheybal, J. Osterwalder, T. A. Jung, Phys. Rev. B **79** (2009) 245421.
9. Ledieu J., Hoeft J. T., Reid D. E., Smerdon J. A., Diehl R. D., Lograsso T. A., Ross A. R., and McGrath R., Phys. Rev. Lett. **92** (2004) 135507.
10. K. Pussi, M. Gierer and R.D. Diehl, J. Phys.: Condens. Matter **21** (2009) 474213.
11. K. M. Young, J. A. Smerdon, H. R. Sharma, M. Lahti, K. Pussi, and R. McGrath, Phys. Rev. B **87** (2013) 085407.
12. G. Kresse, J. Hafner, Phys. Rev. B, **47** (1993) 558.
13. G. Kresse, J. Hafner, J. Phys. Condens. Matter, **6** (1994) 8245.
14. G. Kresse, J. Hafner, Phys. Rev. B, **49** (1994) 14251.
15. G. Kresse, J. Furthmüller, Comput. Mater. Sci., **6** (1996) 15.
16. G. Kresse, J. Furthmüller, Phys. Rev. B, **54** (1996) 11169.
17. P. E. Blöchl, Phys. Rev. B, **50** (1994) 17953.
18. J. P. Perdew, K. Burke, M. Ernzerhof, Phys. Rev. Lett., **77** (1996) 3865.
19. H.J. Monkhorst, J.D. Pack, Phys. Rev. B, **13** (1976) 5188.
20. J. Klimeš, D. R. Bowler, and A. Michaelides, Phys. Rev. B **83** (2011) 195131.
21. H. Yildirim, T. Greber, and A. Kara, J. Phys. Chem. C, **117** (2013) 20572.
22. J. Carrasco, W. Liu, A. Michaelides, A. Tkatchenko, the Journal of Chemical Physics, **140** (2014) 084704.
23. E. Annese, C. E. Viol, B. Zhou, J. Fujii, I. Vobornik, C. Baldacchini, M. G. Betti, and G. Rossi, Surf. Sci. **601** (2007) 4242.
24. J. Lagoute, K. Kanisawa, and S. Fölsch, Phys. Rev. B **70** (2004) 245415.
25. S. Lukas, G. Witte, and C. Wöll, Phys.Rev.Lett. **88** (2001) 028301.
26. J. A. Smerdon, M. Bode, N. P. Guisinger, and J. R. Guest, Phys. Rev. B, **84** (2011) 165436.
27. L. Gross, F. Mohn, N. Moll, P. Liljeroth, and G. Meyer, Science **325** (2009) 1110.
28. K. Müller, A. P. Seitsonen, T. Brugger, J. Westover, T. Greber, T. Jung,and A. Kara, J. Phys. Chem. C, **116** (44) (2012) 23465–23471.
29. J. Carrasco, W. Liu, A. Michaelides and A. Tkatchenko J. Chem. Phys. **140** (2014) 084704.
30. N. Koch, A. Gerlach, S. Duhm, H. Glowatzki, G. Heimel, A. Vollmer, Y. Sakamoto, T. Suzuki, J. Zegenhagen, J. P. Rabe, and F. Schriber, J. Am. Chem. Soc.**130** (2008) 7300.
31. V. Ignatescu, J.-C. M. Hsu, , A. C. Mayer, J. M. Blakely, and G. G. Malliaras, Appl. Phys. Lett. **89**, no. 25 (2006): 253116.
32. C. Baldacchini, M.G. Betti, V. Corradini, and C. Mariani, Surf. Sci. **566**, (2004) pp.613-617.
33. L. Gavioli, M. Fanetti, D. Pasca, M. Padovani, M. Sancrotti, and M.G. Betti, Surf. Sci. **566**, (2004) pp.624-627.
34. I.R. Fisher, M.J. Kramer, T.A. Wiener, Z. Islam, A.R. Ross, T.A. Lograsso, A. Kracher, A.I Goldman, and P.C. Canfield, Phil. Mag. B, **79**(10), (1999) pp.1673-1684.